# Articles

Contribution from the Chemistry Department, Victoria University of Wellington, P.O. Box 600, Wellington, New Zealand, Chemistry Department, University of Canterbury, Christchurch 1, New Zealand, Christopher Ingold Laboratories, University College London, London WC1H 0AJ, England, and Chemistry Department, Queen Mary College, London E1 4NS, England

## A New Polymorph of Tetraphosphorus Triselenide, $\alpha'$-$P_4Se_3$: An X-ray, Raman, and XPS Study of the Normal Crystalline Phases and a DSC Study of the Crystalline and the Orientationally Disordered Phases of $P_4Se_3$

Joanne R. Rollo,[†] Gary R. Burns,*[,†] Ward T. Robinson,[‡] Robin J. H. Clark,[§] Helen M. Dawes,[∥] and Michael B. Hursthouse[∥]

*Received April 25, 1989*

During the course of a detailed crystallographic, spectroscopic, and thermal analysis study of $P_4Se_3$, crystals of a new, room-temperature phase, $\alpha'$-$P_4Se_3$, were isolated. The structure of this phase and that of the normal room-temperature phase, $\alpha$-$P_4Se_3$, have been determined X-ray crystallographically. $\alpha'$-$P_4Se_3$ is orthorhombic, space group *Pnma*, with $a$ = 10.997 (3) Å, $b$ = 9.845 (3) Å, $c$ = 13.803 (5) Å, $V$ = 1494 (4) Å$^3$, $Z$ = 8, and $D_x$ = 3.20 g cm$^{-3}$; $\mu$(Mo K$\alpha$) = 149.8 cm$^{-1}$, $F$(000) = 1296, and $T$ = 133 K. Final $R$ = 0.057 for 956 observed diffractometer data. $\alpha$-$P_4Se_3$ is also orthorhombic, space group *Pnma*, with $a$ = 11.788 (1) Å, $b$ = 9.720 (1) Å, $c$ = 26.254 (2) Å, $V$ = 3008 (1) Å$^3$, $Z$ = 16, and $D_x$ = 3.18 g cm$^{-3}$; $\mu$(Mo K$\alpha$) = 149.8 cm$^{-1}$, $F$(000) = 2592, and $T$ = 265 K. Final $R$ = 0.043 for 1216 observed diffractometer data. The greater thermodynamic stability of $\alpha$-$P_4Se_3$ can be attributed to the formation of double strands of cages in the *ab* plane, with intermolecular Se···Se bonds linking the strands. In $\alpha'$-$P_4Se_3$ there are only single strands of cages and less efficient packing in the unit cell. The Raman-active phonons of the $\alpha$ and $\alpha'$ phases show the expected small differences in the internal mode region, due to the differences in intermolecular bonding, but are significantly different in the external mode region. An XPS study of the crystalline $\alpha$ and $\alpha'$ phase confirms the presence of at least two types of selenium atom in both phases. A DSC study of the phase changes undergone by the newly identified $\alpha'$ phase has helped to clarify the existing literature pertaining to the phases of $P_4Se_3$ and has identified a glass transition and a new orientationally disordered phase.

### Introduction

Tetraphosphorus triselenide is known to exist in at least three crystalline phases: the normal room-temperature form, $\alpha$-$P_4Se_3$, and two higher temperature, orientationally disordered phases, $\beta$-$P_4Se_3$ and $\gamma$-$P_4Se_3$.[1] Detailed Raman studies of $\alpha$-$P_4Se_3$[2-4] have revealed a number of features indicative of intermolecular–intramolecular coupling as observed for elemental selenium.[5] However, analysis of the previously reported structural data[6] did not indicate any unusually short intermolecular contacts. Since the structure of this compound had been determined only from photographic projection data, we considered it worthwhile to refine the structure by using diffractometer data, to see whether possible inaccuracies might be masking fine, but important, structural details. Subsequent to our redetermination of the structure of $\alpha$-$P_4Se_3$, parameters were given by Di Vaira, Peruzzini, and Stoppioni[7] as part of their study of the compound {[N-$(CH_2CH_2PPh_2)_3$]Ni($P_4Se_3$)}·$2C_6H_6$. Their structure, determined at 295 K, gave no analysis of the intermolecular bonding present in crystalline $\alpha$-$P_4Se_3$, which is our prime concern. We give an analysis of the intermolecular bonding and also report the temperature dependence of the unit cell parameters over the temperature range 293–117 K. These data enable us to estimate the coefficient of volume thermal expansion for $\alpha$-$P_4Se_3$ and in addition provide useful evidence on the intermolecular bonding in the crystal.

During the course of the work on $\alpha$-$P_4Se_3$, crystals of a previously unreported crystalline phase, called herein $\alpha'$-$P_4Se_3$, were isolated. The X-ray crystal structure of this new polymorph has been determined, and the Raman and X-ray photoelectron spectra have been measured. The phase changes between the normal crystalline and the orientationally disordered phases have been investigated by using differential scanning calorimetry (DSC).

Characterization of the crystalline phases of $P_4Se_3$ should also help to substantiate the claim[8] that glassy phosphorus–selenium alloys are examples of a "zero-dimensional" glass. The effective density of vibrational states obtained from inelastic neutron-scattering experiments on glassy $P_{0.67}Se_{0.33}$ provides evidence for the existence of molecular clusters based predominantly on $P_4Se_3$ units. The structural studies reported here will allow for the unambiguous identification of the two normal crystalline phases of $P_4Se_3$ and will throw some light on the high-temperature orientationally disordered phases.

### Experimental Section

$\alpha$-$P_4Se_3$. The bulk sample was prepared by refluxing a mixture of yellow phosphorus dissolved in *n*-heptane and selenium, in the presence of a charcoal catalyst.[9] The product was purified by Soxhlet extraction using benzene as solvent, followed by recrystallization from carbon disulfide under an atmosphere of nitrogen.

The structure of this form was determined at Queen Mary College following standard procedures and refined to an $R$ value of 0.043. Since our results are very similar to those obtained by Di Vaira et al., we do not present details of our analysis here but have included a full description, together with coordinates, displacement factor coefficients, bond lengths and angles, and $F_o/F_c$ values, as supplementary material. However, for the discussion of the structure and diagram preparation, we have used our data.

In addition to the structure determination, we have determined the cell dimensions for this phase as a function of temperature, over the range 117–293 K, in order to see whether there is any anisotropy in the coefficient of thermal expansion. A specimen different from that for which intensity data were collected was used. At each temperature a common

* To whom correspondence should be addressed.
† Victoria University of Wellington.
‡ University of Canterbury.
§ University College London.
∥ Queen Mary College.

(1) Blachnik, R.; Wickel, U. *Thermochim. Acta* **1984**, *81*, 185.
(2) Burns, G. R.; Rollo, J. R.; Clark, R. J. H. *Inorg. Chem.* **1986**, *25*, 1145.
(3) Burns, G. R. *J. Phys. Chem. Solids* **1986**, *47*, 681.
(4) Burns, G. R.; Clark, R. J. H. *J. Phys. Chem. Solids* **1986**, *47*, 1049.
(5) Martin, R. M.; Lucovsky, G.; Helliwell, K. *Phys. Rev. B: Condens. Matter* **1976**, *13*, 1383.
(6) Keulen, E.; Vos, A. *Acta Crystallogr.* **1959**, *12*, 323.
(7) Di Vaira, M.; Peruzzini, M.; Stoppioni, P. *J. Organomet. Chem.* **1983**, *258*, 373.
(8) Verrall, D. J.; Elliott, S. R. *Phys. Rev. Lett.* **1988**, *61*, 974.
(9) Irgolic, K.; Zingaro, R. A.; Kudchadker, M. *Inorg. Chem.* **1965**, *4*, 1421.

0020-1669/90/1329-2889$02.50/0 

**Table I.** Atomic Fractional Coordinates ($\times 10^4$) and Isotropic Temperature Factors ($Å^2 \times 10^3$) for the $\alpha'$-$P_4Se_3$ Asymmetric Unit

| atom | x | y | z | $U^a$ |
|---|---|---|---|---|
| Se(1′) | −5567 (1) | 761 (2) | 8665 (1) | 52 (1) |
| Se(3′) | −3311 (2) | 2500 | 9812 (1) | 47 (1) |
| P(1′) | −4270 (4) | 1377 (4) | 7503 (3) | 53 (1) |
| P(3′) | −2781 (4) | 2500 | 8246 (4) | 54 (2) |
| P(4′) | −5331 (4) | 2500 | 9696 (3) | 41 (2) |
| Se(1) | −1538 (1) | 5769 (2) | 9777 (1) | 47 (1) |
| Se(3) | 674 (2) | 7500 | 8554 (1) | 48 (1) |
| P(1) | −2379 (3) | 6371 (4) | 8375 (3) | 48 (1) |
| P(3) | −948 (5) | 7500 | 7584 (4) | 55 (2) |
| P(4) | −241 (4) | 7500 | 9999 (3) | 40 (2) |

[a] Equivalent isotropic $U$ defined as one-third of the trace of the orthogonalized $U_{ij}$ tensor.

set of 25 well-spaced reflections was recentered and cell dimensions were obtained by least-squares analysis on setting angles.

**$\alpha'$-$P_4Se_3$.** Crystals of $\alpha'$-$P_4Se_3$ were obtained by adding petroleum ether to a solution of $P_4Se_3$ dissolved in carbon disulfide until the solution just became turbid. Large, dark red crystals formed after several days and were removed by vacuum filtration and stored in a desiccator. The crystal used for the X-ray work was a small irregular red crystal [maximum dimension 0.2 mm, orthorhombic, $a$ = 10.997 (3) Å, $b$ = 9.845 (3) Å, $c$ = 13.803 (5) Å, $V$ = 1494 (4) Å$^3$, space group *Pnma*, $Z$ = 8, $F(000)$ = 1296]. With Mo K$\alpha$ radiation, 2.0° $\omega$-scans at a scan rate of 4.88° min$^{-1}$, and a background-to-scan ratio of 0.25, 2064 reflections were collected for $5 < 2\theta < 50°$, at 133 K. Of these, 1488 were unique, and 956 having $I > 3\sigma(I)$ were ultimately used in the structure refinement.

The cell parameters were determined by least-squares refinement using 25 accurately centered reflections in the range $18 < 2\theta < 32°$. Crystal stability was monitored by recording three check reflections every 100 reflections, and no significant variations were observed. The data were corrected for Lorentz and polarization effects, and an empirical absorption correction based on $\psi$-scans was applied [$\mu$(Mo K$\alpha$) = 153.6 cm$^{-1}$, $T_{max}$ = 0.999 K, $T_{min}$ = 0.181 K].

Atomic coordinates were taken from the isomorphous $P_4S_3$ structure,[10] and anisotropic thermal parameters were assigned to all atoms. Least-squares refinement on 73 parameters converged with $R$ = 0.0571, $R_w$ = 0.0602, and a maximum least-squares shift/error of 0.006. The final difference map showed no features greater than ±1.13 e Å$^{-3}$. The function minimized in the refinement was $\sum w(|F_o| - |F_c|)^2$ where $w = [\sigma^2(F_o) + 0.0024F_o^2]^{-1}$.

**Raman Spectroscopy.** Raman spectra were recorded on a Spex 1401 double monochromator in conjunction with a Spectra Physics Model 164-01 krypton ion laser. Detection of the radiation was by standard photon-counting techniques using a thermoelectrically cooled RCA C31034A photomutiplier tube. Wavenumber measurements were calibrated by reference to the emission spectrum of neon.

**Differential Thermal Analysis.** Differential thermal analysis was performed by using a Perkin-Elmer differential scanning calorimeter (DSC-2C) with an Intracooler II refrigeration unit and a Perkin-Elmer thermal analysis data station. The energy and temperature scales of the calorimeter were calibrated from the enthalpies of fusion and the melting points of indium and benzoic acid. Samples of $\alpha'$-$P_4Se_3$ of approximately 16 mg were transferred to aluminum sample pans, sealed, weighed, and loaded into the calorimeter. The scanning rate used was 10 K min$^{-1}$.

**X-ray Photoelectron Spectra.** XPS data were gathered with a Kratos XSAM 800 XPS/Auger spectrometer. Mg K$\alpha$ ($h\nu$ = 1253.6 eV) was used as the X-ray source, and the analyzer was operated at a constant pass energy of 20 eV. Curve fitting was carried out with the standard DS800 software of the XSAM 800 spectrometer. Samples were ground into a powder and spread onto indium foil immediately before being introduced into the spectrometer. All XPS spectra were calibrated with respect to the $C_{1s}$ line from adsorbed hydrocarbon, this line being assumed to occur at 285.0 eV.[11]

## Results

**Crystallography.** The positional and thermal parameters of the asymmetric unit for $\alpha'$-$P_4Se_3$ are given in Table I, and the intramolecular bond lengths and angles are given in Table II. A diagram of one of the crystallographically independent molecules in the unit cell is given in Figure 1, and views of the unit cell contents for both $\alpha$- and $\alpha'$-$P_4Se_3$ are given in Figures 2 and 3, respectively.

**Table II.** Bond Lengths and Bond Angles for $\alpha'$-$P_4Se_3$

| Bond Lengths (Å) | | | |
|---|---|---|---|
| Se(1′)-P(1′) | 2.230 (4) | Se(1′)P(4′) | 2.241 (3) |
| Se(3′)-P(3′) | 2.238 (6) | Se(3′)-P(4′) | 2.227 (5) |
| P(1′)-P(3′) | 2.226 (6) | P(1′)-P(1′a) | 2.212 (8) |
| P(3′)-P(1′a) | 2.226 (6) | P(4′)-Se(1a) | 2.242 (3) |
| Se(1)-P(1) | 2.225 (4) | Se(1)-P(4) | 2.243 (3) |
| Se(3)-P(3) | 2.231 (6) | Se(3)-P(4) | 2.234 (5) |
| P(1)-P(3) | 2.214 (6) | P(1)-P(1a) | 2.223 (8) |
| P(3)-P(1a) | 2.214 (6) | P(4)-Se(1b) | 2.243 (3) |

| Bond Angles (deg) | | | |
|---|---|---|---|
| P(1′)-Se(1′)-P(4′) | 100.1 (2) | P(3′)-Se(3′)-P(4′) | 101.0 (2) |
| Se(1′)-P(1′)-P(3′) | 105.9 (2) | Se(1′)-P(1′)-P(1′a) | 105.8 (1) |
| P(3′)-P(1′)-P(1′a) | 60.2 (1) | Se(3′)-P(3′)-P(1′) | 104.7 (2) |
| Se(3′)-P(3′)-P(1′a) | 104.7 (2) | p(1′)-P(3′)-P(1′a) | 59.6 (2) |
| Se(1′)-P(4′)-Se(3′) | 99.3 (2) | Se(1′)-P(4′)-Se(1a) | 99.6 (2) |
| Se(3′)-P(4′)-Se(1a) | 99.3 (2) | P(1)-Se(1)-P(4) | 100.4 (2) |
| P(3)-Se(3)-P(4) | 100.1 (2) | Se(1)-P(1)-P(3) | 105.5 (2) |
| Se(1)-P(1)-P(1a) | 105.5 (1) | P(3)-P(1)-P(1a) | 59.9 (1) |
| Se(3)-P(3)-P(1) | 105.8 (2) | Se(3)-P(3)-P(1a) | 105.8 (2) |
| P(1)-P(3)-P(1a) | 60.3 (3) | Se(1)-P(4)-Se(3) | 99.5 (1) |
| Se(1)-P(4)-Se(1b) | 98.9 (2) | Se(3)-P(4)-Se(1b) | 99.5 (1) |

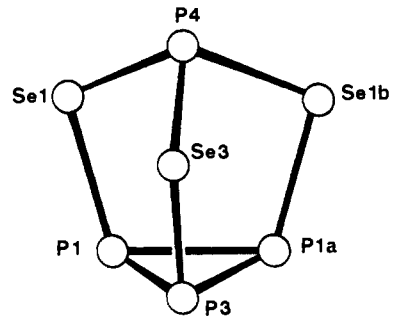


**Figure 1.** Molecular structure and atomic nomenclature for $\alpha'$-$P_4Se_3$.

For $\alpha$-$P_4Se_3$, the four crystallographically independent molecules lie on mirror planes, but the molecular symmetry approximates closely to $C_{3v}$, with all chemically equivalent bonds having equal lengths within the limits of experimental error. There are a number of Se···Se and P···Se intermolecular contacts significantly shorter than the sum of the individual van der Waals radii for P and Se. Significant Se···Se contacts range from 3.625 (6) to 3.798 (6) Å within strands of helices, and there are Se···Se and P···Se contacts of 3.771 (6) and 3.653 (7) Å, respectively, which link adjacent strands.

The changes in unit cell parameters for $\alpha$-$P_4Se_3$, measured over the temperature range 293–117 K, are given in Table III, and the linear expansions along the cell axes are shown in Figure 4. When temperature decreases, $\alpha_a$ remains nearly constant whereas $\alpha_b$ decreases rapidly and $\alpha_c$ decreases slowly. The coefficient of volume thermal expansion decreases slowly and linearly from its room-temperature value ($\alpha_V$(293 K) = 1.80 (5) × 10$^{-4}$ K$^{-1}$) down to 117 K.

The new polymorph, $\alpha'$-$P_4Se_3$, is isomorphous with $\alpha$-$P_4S_3$, the only known ordered crystalline polymorph of $P_4S_3$. The intramolecular bond lengths and angles found for $\alpha'$-$P_4Se_3$ do not differ significantly from those in $\alpha$-$P_4Se_3$. However, there are differences in the intermolecular contact distances. The shortest intermolecular Se···Se contact is 3.673 (7) Å between Se(3) and Se(3′). Distances of 3.76 Å (Se(1)···Se(3′)), 3.59 Å (Se(3)···P(1)), and 3.84 Å (Se(1)···Se(1′)) are also observed. The cell parameters for the $\alpha'$-$P_4Se_3$ unit cell also differ significantly from those observed for $\alpha$-$P_4Se_3$. The $c$ axis for $\alpha$-$P_4Se_3$ is double that for $\alpha'$-$P_4Se_3$, and so it is convenient to compare the $\alpha'$ cell with the $a \times b \times {}^1/_2c$ (equivalent) cell for $\alpha$-$P_4Se_3$. For the equivalent cell, there are increases in the $b$ and $c$ cell axes and a small increase in the volume but a large decrease in the $a$ axis on going from the $\alpha$ to the $\alpha'$ structure.

(10) Leung, Y. C.; Waser, J.; van Houten, S.; Vos, A.; Wiegers, G. A.; Wiebenga, E. H. *Acta Crystallogr.* **1957**, *10*, 574.
(11) Gelius, U.; Heden, P. F.; Hedman, J.; Lindberg, B. J.; Manne, R.; Nordberg, R.; Nordling, C.; Siegbahn, K. *Phys. Scr.* **1970**, *2*, 70.

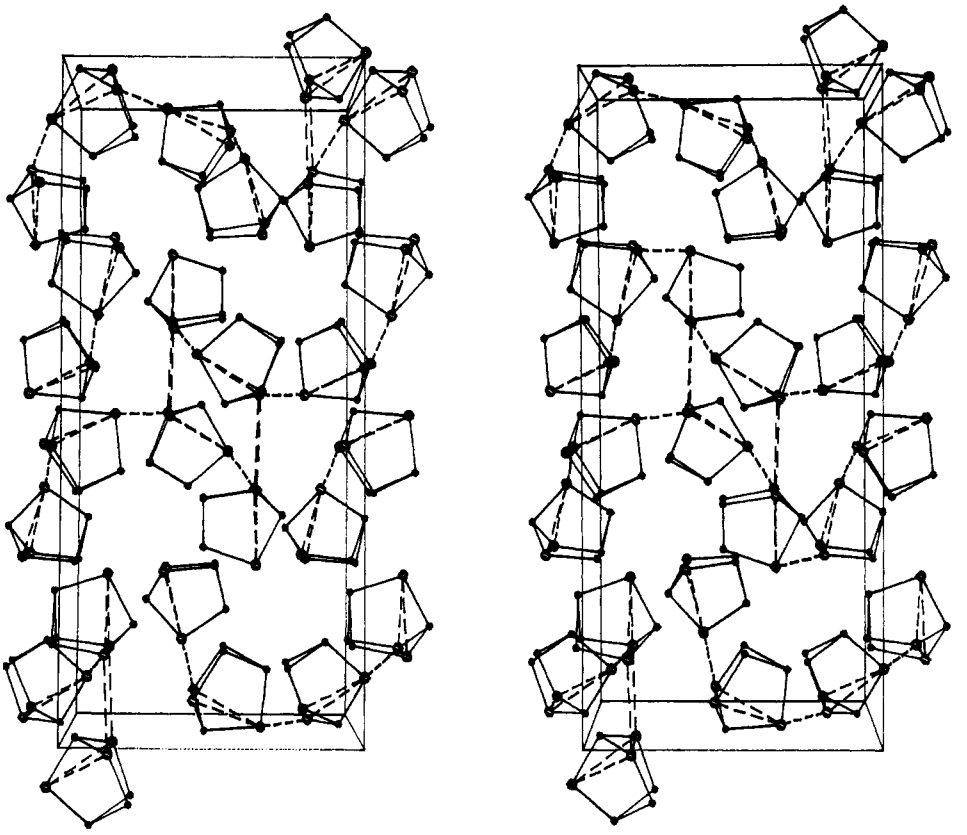

**Figure 2.** Projection of the unit cell for $\alpha$-$P_4Se_3$ along the [010] direction.

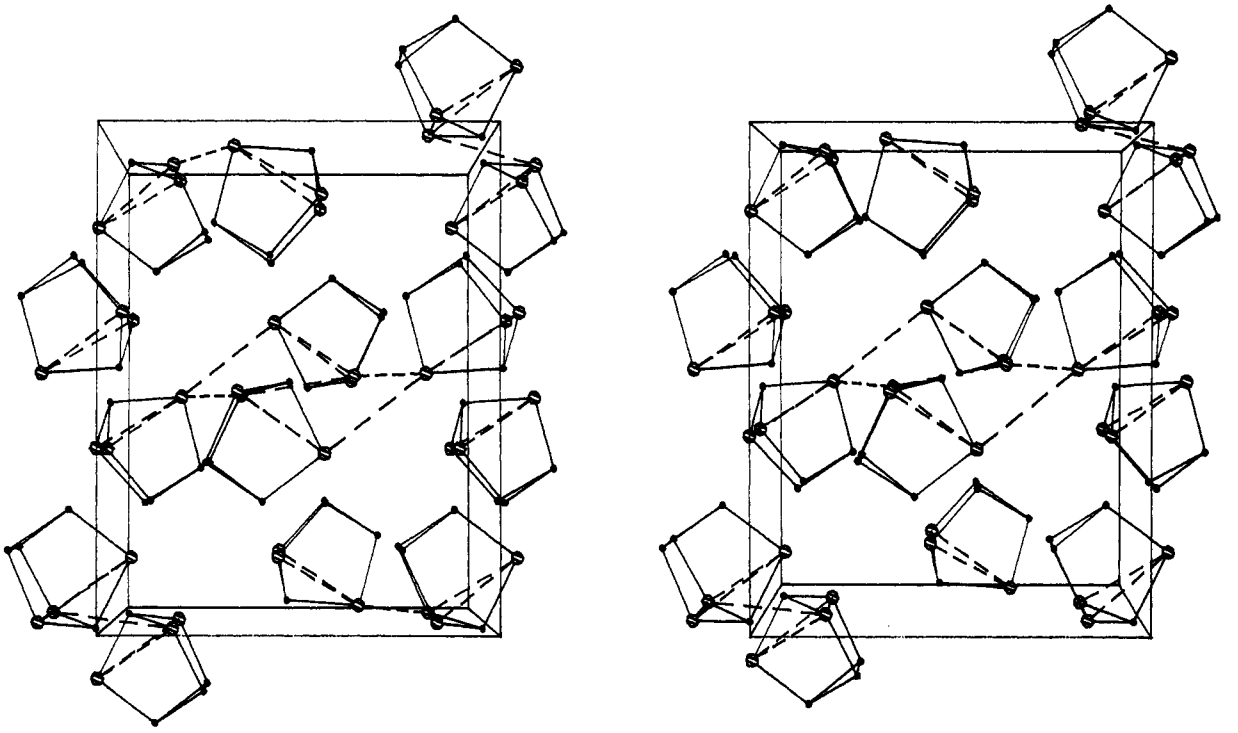

**Figure 3.** Projection of the unit cell for $\alpha'$-$P_4Se_3$ along the [010] direction.

**Table III.** Temperature Dependence of Unit Cell Parameters for $\alpha$-$P_4Se_3$[a]

| | $T$/K | | | | | | | |
|---|---|---|---|---|---|---|---|---|
| | 293 | 270 | 243 | 216 | 189 | 162 | 135 | 117 |
| $a$/Å | 11.783 | 11.770 | 11.762 | 11.752 | 11.742 | 11.733 | 11.723 | 11.717 |
| $b$/Å | 9.730 | 9.697 | 9.677 | 9.658 | 9.639 | 9.627 | 9.612 | 9.601 |
| $c$/Å | 26.259 | 26.223 | 26.211 | 26.188 | 26.161 | 26.157 | 26.142 | 26.131 |
| $V$/Å$^3$ | 3010.5 | 2993.0 | 2983.4 | 2972.4 | 2960.9 | 2954.3 | 2945.7 | 2939.8 |

[a] ESD's in the cell dimensions were 0.002 Å for $a$ and $b$ and 0.003 Å for $c$. The uncertainty in the temperatures is ±2 K.

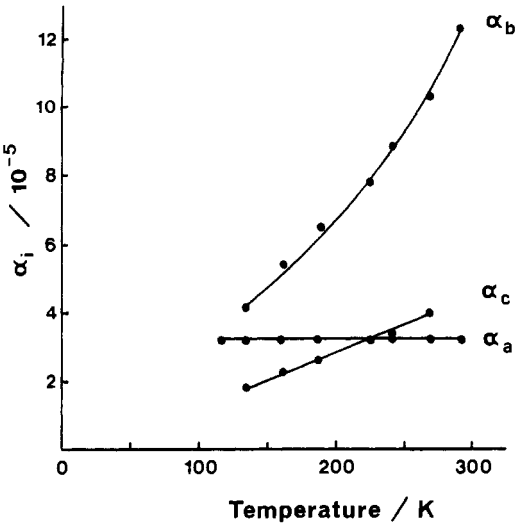


**Figure 4.** Linear expansions along the cell axes for $\alpha$-$P_4Se_3$.

**Table IV.** Observed Wavenumbers ($cm^{-1}$) for Raman Bands of Crystalline $\alpha'$-$P_4Se_3$, $\alpha$-$P_4Se_3$, and $\alpha$-$P_4S_3$ Measured at 295 K

| $\alpha'$-$P_4Se_3$ | $\alpha$-$P_4Se_3$ | $\alpha$-$P_4S_3$ |
|---|---|---|
| 22.5 | 12.4 | 27 |
| 25.8 | 23 | 30 |
| 33.1 | 27.0 | 36 |
| 45.8 | 33.2 | 46 |
| 49.9 | 36.6 | 58 |
| 59.4 | 46.0 | 72 |
| | 53.2 | |
| 130.8 | | |
| 133.0 | 134.5 | |
| 137.2 | | |
| 154.9 | | |
| | 209.4 | |
| 210.5 | 213.2 | |
| 214.9 | 216 | |
| 218.3 | 218.8 | |
| 315.5 | 315.6 | |
| 322.8 | 323.9 | |
| 358.8 | | |
| 360.8 | 361.0 | |
| 365.8 | 365.0 | |
| | 371.8 | |
| 405.0 | 404.8 | |
| 483.3 | 483.8 | |
| | 486.4 | |

**Raman Spectra.** The phonon wavenumbers observed in the Raman spectrum of $\alpha'$-$P_4Se_3$ at room temperature are given in Table IV. The room-temperature Raman data for $\alpha$-$P_4Se_3$ and the lattice modes of $\alpha$-$P_4S_3$ have been included for comparison. The $\alpha$ and $\alpha'$ spectra are similar in the internal mode region with only one new weak band appearing for $\alpha'$ at 154.2 $cm^{-1}$. The 132-$cm^{-1}$ band (Figure 5), which appears in the room-temperature spectrum of $\alpha$-$P_4Se_3$ as a single unresolved feature, is replaced by a doublet in the room-temperature spectrum of $\alpha'$-$P_4Se_3$. The most intense band in the spectrum of $\alpha'$-$P_4Se_3$ (Figure 6) occurs at 361.6 $cm^{-1}$, and there is a slightly weaker band at 366.0 $cm^{-1}$. For $\alpha$-$P_4Se_3$, the 365-$cm^{-1}$ band is more intense and there is an additional band at 371 $cm^{-1}$.

In the external mode region, the Raman active modes for the new $\alpha'$ phase are significantly different from those of $\alpha$-$P_4Se_3$. As observed previously,[2] there is no simple scaling relation between the lattice modes for $\alpha$-$P_4Se_3$ and $\alpha$-$P_4S_3$. However, a comparison of the Raman-active lattice modes for $\alpha'$-$P_4Se_3$ and $\alpha$-$P_4S_3$ shows that such a scaling factor, or factors, do exist. From the data reported in Table IV, two phonons have scaling factors of 0.72 (2) and three have values of 0.80 (2). The smaller value may reflect lattice modes involving the intrachain-coupled selenium atoms. A similar scaling relationship has been noted for the isomorphous crystals $As_2S_3$ and $As_2Se_3$.[12]

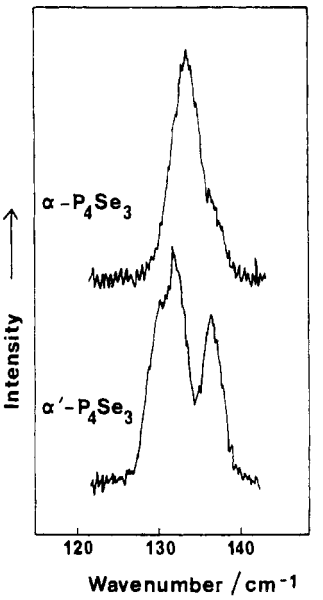


**Figure 5.** Phonon structure centered at 134 $cm^{-1}$ in the Raman spectra of $\alpha'$-$P_4Se_3$ and $\alpha$-$P_4Se_3$.

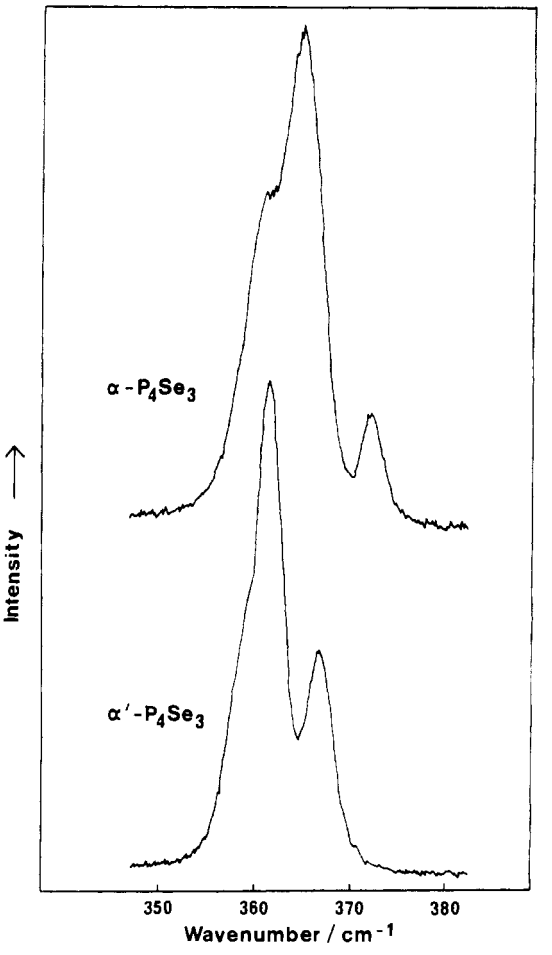


**Figure 6.** Phonon structure centered at 365 $cm^{-1}$ in the Raman spectra of $\alpha'$-$P_4Se_3$ and $\alpha$-$P_4Se_3$.

In general, the Raman-active phonons of $\alpha'$-$P_4Se_3$ all display regular dependences on temperature. However, at temperatures of 355 ± 5 K and above, the complete loss of the external mode manifold and a discontinuity in $(d\nu/dT)_p$ for the internal modes centered at 212 and 360 $cm^{-1}$ are observed. This is consistent with a phase transition to the orientationally disordered state,

(12) Zallen, R.; Slade, M. *Phys. Rev. B: Condens. Matter* **1974**, *9*, 1627.

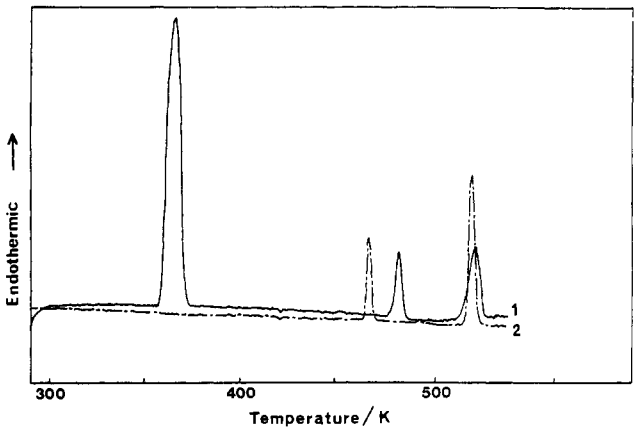


**Figure 7.** DSC behavior of $\alpha'$-$P_4Se_3$ during heating experiments over the temperature range 220–545 K: (1) first heating (—); (2) second and subsequent heatings (- — -).

**Table V.** Thermodynamic Data for the Phase Changes for $\alpha'$-$P_4Se_3$

| | $\alpha' \leftrightarrow \beta$ | $\beta \leftrightarrow \gamma$ | $\gamma \leftrightarrow$ melt |
|---|---|---|---|
| | Heating Cycle 1 | | |
| $T$/K | 358 ± 0.5 | 480 ± 0.5 | 517 ± 0.5 |
| $\Delta H$/kJ mol$^{-1}$ | 11.35 ± 0.57 | 1.30 ± 0.07 | 2.36 ± 0.12 |
| | Cooling Cycle 1 | | |
| $T$/K | | 424 | 516 |
| $\Delta H$/kJ mol$^{-1}$ | | 1.13 ± 0.06 | 2.77 ± 0.13 |
| | Heating Cycle 2 | | |
| $T$/K | | 465 | 519 |
| $\Delta H$/kJ mol$^{-1}$ | | 2.55 ± 0.13 | 2.38 ± 0.12 |
| | Cooling Cycle 2 | | |
| $T$/K | | 424 | 516 |
| | Heating Cycle 3 | | |
| $T$/K | | 465 | 519 |

$\beta$-$P_4Se_3$. When $\beta$-$P_4Se_3$ cools, $\alpha'$-$P_4Se_3$ is not re-formed; rather, the $\alpha$ phase is formed. This transformation has been confirmed by DSC and by X-ray powder diffraction.

**Differential Scanning Calorimetry.** The DSC results for $\alpha'$-$P_4Se_3$ are shown in Figure 7, and the data are summarized in Table V. The phases observed during a heating and cooling cycle depend on sample history. If the $\alpha'$ phase is taken into the liquid phase at a heating rate of 10 K min$^{-1}$, three phase changes are observed, as previously reported.[1] However, the behavior on subsequent cooling and heating cycles observed in this study differs from that reported by earlier workers.[1,13] Some of the confusion in the earlier work can be attributed to the nonrecognition of an $\alpha'$ phase.

As the melt cools, a large hysteresis is observed for the $\gamma \rightarrow \beta$ transition and no $\beta \rightarrow \alpha$ transition is observed. Instead, there is a glass transition observed at 230 K for subsequent heating cycles. In addition, on subsequent heating cycles the $\beta \rightarrow \gamma$ transition occurs at 466 K rather than at the first-cycle value of 480 K, implying some new orientationally disordered phase.

The transformations between the orientationally ordered and disordered phases were investigated further by scanning different intervals within the temperature range 250–550 K.

When $\alpha'$-$P_4Se_3$ is heated from 250 to 400 K, the $\alpha'$-$P_4Se_3 \rightarrow$ $\beta$-$P_4Se_3$ transformation occurs at 358 ± 0.5 K. Cooling from 400 to 250 K reveals two peaks; one transition is observed at 335 K, with $\Delta H$ = 10.1 ± 0.5 kJ mol$^{-1}$, and a second transition is observed at 322 K, with $\Delta H$ = 0.42 ± 0.02 kJ mol$^{-1}$. It appears that orientationally ordered phases crystallize from the $\beta$ phase. Raman and XRD studies show that when the $\alpha'$ phase is converted to orientationally disordered $\beta$-$P_4Se_3$ and then cooled, only the $\alpha$ phase is obtained.

When the same sample is heated over the temperature interval 250–500 K, the $\alpha \rightarrow \beta$ transformation occurs at 356 K, and the $\beta \rightarrow \gamma$ transformation occurs at 480 K. Cooling over this same temperature range reveals the $\gamma \rightarrow \beta$-$P_4Se_3$ transition at 440 K. A broad peak at ≈302 K may correspond to the crystallization of a remnant orientationally ordered phase from the $\beta$ phase.

Finally, heating the same sample over the temperature interval 250–550 K reveals a broad peak from 317 to 336 K for the $\alpha \rightarrow \beta$ phase transformation, the $\beta \rightarrow \gamma$ transformation peak at 468 K, and the $\gamma \rightarrow$ melt transformation peak at 514 K. The cooling cycle, and a subsequent heating cycle to 550 K, gave results identical with those reported in Table V for the heating and cooling cycles over the extended range.

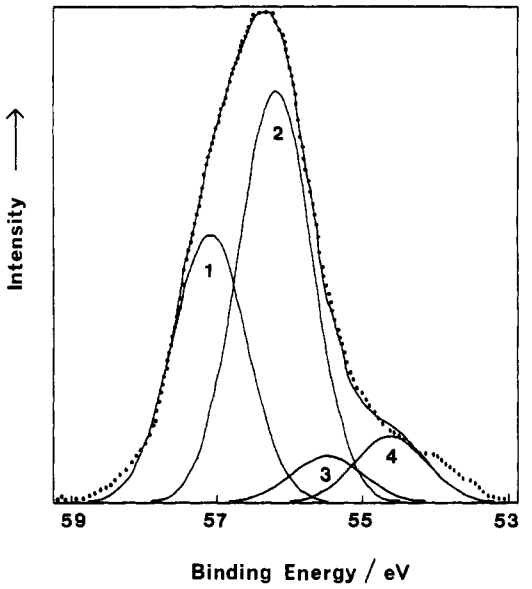


**Figure 8.** Selenium 3d XPS spectra of $\alpha$-$P_4Se_3$: (···) raw spectrum after smoothing; (—) four-peak Gaussian fit. 1–4 refer to Se(coupled $3d_{3/2}$), Se(coupled $3d_{5/2}$), Se(noncoupled $3d_{3/2}$), and Se(noncoupled $3d_{5/2}$).

**Table VI.** XPS Data for $\alpha$-$P_4Se_3$ and $\alpha'$-$P_4Se_3$ in Terms of the Binding Energy (BE) and the Peak Area for Each Type of Selenium Atom

| | coupled Se | | noncoupled Se | | |
|---|---|---|---|---|---|
| | BE/eV | area | BE/eV | area | diff in BE/eV |
| | | | $\alpha$-$P_4Se_3$ | | |
| $3d_{3/2}$ | 57.2 | 33.1 | 55.6 | 5.6 | 1.6 |
| $3d_{5/2}$ | 56.3 | 50.9 | 54.7 | 8.1 | 1.6 |
| | | | $\alpha'$-$P_4Se_3$ | | |
| $3d_{3/2}$ | 56.9 | 35.2 | 55.7 | 4.0 | 1.2 |
| $3d_{5/2}$ | 56.0 | 52.2 | 54.8 | 6.1 | 1.2 |

**X-ray Photoelectron Spectra.** Figure 8 shows the $Se_{3d}$ lines for $\alpha$-$P_4Se_3$. It was necessary to use a four-peak fit to account for the observed $Se_{3d}$ line shape, and this implies the presence of two types of selenium atoms in the $\alpha$-$P_4Se_3$ crystal: those involved in strong intramolecular–intermolecular coupling and those which are intramolecularly bonded only. The shoulder that occurs at the lower binding energy side of the $Se_{3d}$ peak can be tentatively assigned to noncoupled selenium atoms. The lower binding energy results from a higher electron density on these atoms. For the coupled selenium atoms, electron density is shared over more atomic centers and hence the binding energy is slightly higher.

The peak splitting between coupled and noncoupled selenium atoms is approximately 1.6 ± 0.1 eV. A similar splitting of the $Se_{3d}$ line has been observed for $As_2Se_3$–$Tl_2Se$ glasses.[14] In this case the splitting has been ascribed to the presence of bridging and nonbridging selenium atoms.

Table VI shows a summary of the experimental results for both $\alpha$-$P_4Se_3$ and $\alpha'$-$P_4Se_3$.

The selenium XPS spectra of $\alpha'$-$P_4Se_3$ were measured in the hope that differences in intermolecular bonding between the two

(13) Sanghera, J. S.; Heo, J.; MacKenzie, J. D.; Almeida, R. M. *J. Non-Cryst. Solids* **1988**, *101*, 18.

(14) Monteil, Y.; Vincent, H. *Z. Anorg. Allg. Chem.* **1975**, *416*, 181.

phases, $\alpha$ and $\alpha'$, would be revealed.

Splitting of the $Se_{3d}$ lines was observed, indicative of the presence of coupled and noncoupled selenium atoms. The splitting of the $Se_{3d}$ peaks (1.2 ± 0.1 eV) is slightly less than that observed for $\alpha$-$P_4Se_3$. The smaller splitting suggests that the difference between coupled and noncoupled selenium atoms is less distinct than in $\alpha$-$P_4Se_3$. The binding energies and the electron densities on the noncoupled selenium atoms are approximately the same in $\alpha$- and $\alpha'$-$P_4Se_3$. The binding energy of the coupled selenium atoms in $\alpha'$-$P_4Se_3$ is slightly lower than that in $\alpha$-$P_4Se_3$. From this it may be concluded that the electron density on the coupled selenium atoms in $\alpha'$-$P_4Se_3$ is slightly higher than on the coupled selenium atoms in $\alpha$-$P_4Se_3$, implying that there is less delocalization of electrons between $\alpha'$-$P_4Se_3$ molecules. This in turn implies that the coupling between molecules is weaker in the $\alpha'$ phase.

## Discussion

The structure of $\alpha$-$P_4Se_3$ can be described as consisting of layers of double-stranded helices. Each helix, lying orthogonal to the long $c$ axis of the unit cell, is composed of intermolecularly bonded cages in which Se···Se and some P···Se contacts are important. In $\alpha'$-$P_4Se_3$, the individual helices are retained but are no longer paired due to a different orientation for alternate helices along the $c$ direction. This different packing has P···P and P···Se interactions separating the layers. The changes in the unit cell dimensions reflect these differences in that for the equivalent $\alpha$ cell ($a \times b \times {}^1/_2c$), there is an increase of 5.6% in $c$, a comparable decrease of 6.2% in $a$, and a small increase of 2.4% in $b$ on going from $\alpha$ to $\alpha'$. This can be interpreted as indicating a weakening of the intermolecular bonding along the $c$ direction as the Se···Se interaction, giving rise to the double-stranded structure, is replaced by the weaker P···P interaction. There is a concomitant strengthening of the intermolecular bonding in the 001 plane. This parallels the changes observed for selenium chains in mordenite, a zeolite matrix. An EXAFS study[15] showed that the nearest Se–Se distance in selenium chains is shortened compared to the value in trigonal selenium. The covalent bond along the chain becomes stronger when coupling between adjacent chains is inhibited.

The temperature dependence of the unit cell parameters for $\alpha$-$P_4Se_3$ is also informative about the intermolecular bonding. A comparison of the observed changes (Table IV) with those previously reported[16] for $\alpha$-$P_4S_3$ shows that the changes in $b$ and $c$ are similar whereas the change in $a$ is only about half that observed in the sulfide crystal. If this reflects stronger intermolecular bonding in the selenide, then it supports the earlier observation[4,17] of stronger intermolecular–intramolecular coupling for $\alpha$-$P_4Se_3$ compared to $\alpha$-$P_4S_3$.

The small but measurable differences between the lattices for $\alpha$- and $\alpha'$-$P_4Se_3$ are confirmed by the Raman and XPS spectra of the two crystals. In the case of the XPS data, it has been possible to identify the presence of two distinct types of selenium atom, differing in terms of the extent to which they are involved in strong intermolecular Se···Se bonding.

**Acknowledgment.** Dr. A. R. MacGibbon, Dairy Research Institute, Palmerston North, New Zealand, is thanked for help in obtaining the DSC data, and J.R.R. thanks the UGC for the award of a postgraduate scholarship, during the tenure of which this work was completed.

**Registry No.** $P_4Se_3$, 1314-86-9; $P_4S_3$, 1314-85-8.

**Supplementary Material Available:** A textual summary of the structural determination and tables of atomic fractional coordinates, anisotropic temperature factors, bond lengths and angles, and selected nonbonded distances for $\alpha$-$P_4Se_3$ and anisotropic temperature factors for $\alpha'$-$P_4Se_3$ (6 pages); listings of structure factors for $\alpha$-$P_4Se_3$ and $\alpha'$-$P_4Se_3$ (11 pages). Ordering information is given on any current masthead page.

(15) Tamura, K.; Hosokawa, S.; Endo, H.; Yamasaki, S.; Oyanagi, H. *J. Phys. Soc. Jpn.* **1986**, *55*, 528.

(16) Chattopadhyay, T. K.; May, W.; von Schnering, H. G.; Pawley, G. S. *Z. Kristallogr.* **1983**, *165*, 47.

(17) Burns, G. R.; Rollo, J. R. *J. Phys. Chem. Solids* **1987**, *48*, 347.

Contribution from the Department of Chemistry, Princeton University, Princeton, New Jersey 08544-1009

# Nickel-Electrode-Confined $\{Ru(bipyrazine)_3[Fe(CN)_5]_n\}^{2-3n}$: An Inorganic Structural Matrix Yielding Photoinduced Multinuclear Charge-Transfer Reactivity

Carmela Hidalgo-Luangdilok and Andrew B. Bocarsly*,†

*Received August 8, 1989*

The complex $\{Ru(bpz)_3[Fe(CN)_5]_n\}^{2-3n}$ (where $n$ = 1–6 and bpz ≡ bipyrazine) containing a central ruthenium(II) and an overall octahedral site symmetry can be surface-attached to a variety of electrodes via reaction with electrogenerated nickel ions. The well-defined geometry of this complex allows it to be considered as a "molecular building block" for the construction of microstructure-specific chemically derivatized interfaces. In addition to exhibiting a sophisticated interfacial structure, this class of electrodes is found to yield both photocathodic and photoanodic currents under illumination in an aqueous electrolyte. The photocurrent is found to be molecular in nature and can be explained in terms of charge-transfer quenching of a Ru(II) → bpz charge-transfer excited state by the pendant pentacyanoferrate groups. Excitation and quenching events appear to be highly localized. The sense of the photocurrent is controlled by the initial oxidation state of the surface-confined iron. Under conditions yielding a photocathodic current, the charge is eventually consumed by the reduction of dissolved $O_2$.

## Introduction

A variety of approaches have been developed for the attachment of chromophores to electrode surfaces. Among these is the use of polymer and polyelectrolyte coatings, which can readily incorporate various ionic electroactive species such as $Ru(bpy)_3^{2+}$ (bpy = bipyridine) into their matrices.[1] Using this approach, modification of semiconductor electrode surfaces with $Ru(bpy)_3^{2+}$ in many cases has led to the observation of a photoresponse that is attributed to the quenching of the metal-to-ligand charge-transfer (MLCT) excited state of $Ru(bpy)_3^{2+*}$ by quenchers

* To whom correspondence should be addressed.
† Alfred P. Sloan Fellow, 1986–1988.

(1) (a) Oyama, N.; Anson, F. C. *J. Am. Chem. Soc.* **1979**, *101*, 739. (b) Oyama, N.; Anson, F. C. *J. Electrochem. Soc.* **1980**, *127*, 247. (c) Oyama, N.; Shimomura, K.; Shigehara, K.; Anson, F. C. *J. Electroanal. Chem. Interfacial Electrochem.* **1980**, *112*, 271. (d) Rubinstein, I.; Bard, A. J. *J. Am. Chem. Soc.* **1980**, *102*, 6641. (e) Rubinstein, I.; Bard, A. J. *J. Am. Chem. Soc.* **1981**, *103*, 5007.

0020-1669/90/1329-2894$02.50/0 